# High density liquid structure enhancement in glass forming aqueous solution of LiCl

G. Camisasca, M. De Marzio, M. Rovere, and P. Gallo

Citation: The Journal of Chemical Physics **148**, 222829 (2018); doi: 10.1063/1.5024375
View online: https://doi.org/10.1063/1.5024375
View Table of Contents: http://aip.scitation.org/toc/jcp/148/22
Published by the American Institute of Physics

# High density liquid structure enhancement in glass forming aqueous solution of LiCl

G. Camisasca, M. De Marzio, M. Rovere, and P. Gallo
*Dipartimento di Matematica e Fisica, Università "Roma Tre," Via della Vasca Navale 84, 00146 Roma, Italy*

(Received 31 January 2018; accepted 27 March 2018; published online 17 April 2018)

We investigate using molecular dynamics simulations the dynamical and structural properties of LiCl:6$H_2O$ aqueous solution upon supercooling. This ionic solution is a glass forming liquid of relevant interest in connection with the study of the anomalies of supercooled water. The LiCl:6$H_2O$ solution is easily supercooled and the liquid state can be maintained over a large decreasing temperature range. We performed simulations from ambient to 200 K in order to investigate how the presence of the salt modifies the behavior of supercooled water. The study of the relaxation time of the self-density correlation function shows that the system follows the prediction of the mode coupling theory and behaves like a fragile liquid in all the range explored. The analysis of the changes in the water structure induced by the salt shows that while the salt preserves the water hydrogen bonds in the system, it strongly affects the tetrahedral hydrogen bond network. Following the interpretation of the anomalies of water in terms of a two-state model, the modifications of the oxygen radial distribution function and the angular distribution function of the hydrogen bonds in water indicate that LiCl has the role of enhancing the high density liquid component of water with respect to the low density component. This is in agreement with recent experiments on aqueous ionic solutions. *Published by AIP Publishing.*
https://doi.org/10.1063/1.5024375

## I. INTRODUCTION

The anomalous behavior of water is strongly enhanced in the supercooled state.[1,2] The strong increase of thermodynamic response functions, such as the isothermal compressibility, the isobaric specific heat, and the negative coefficient of thermal expansion, upon supercooling has been for long time extrapolated to a divergent behavior that at ambient pressure would take place at a singular temperature $T \sim 238$ K (−42 °C). Different interpretations of this anomalous behavior have been proposed over the years. The first scenario was the so-called stability limit conjecture hypothesized by Speedy.[3] Some years later, Poole, Sciortino, Essmann, and Stanley[4] on the basis of computer simulation proposed that in supercooled water it can be a phase coexistence between a low density liquid (LDL) phase and a high density liquid (HDL) phase. The coexistence curve would be the continuation of the first order phase transition line that exists between the low density amorphous (LDA) ice and the high density amorphous (HDA) ice, already known from experiments.[1] In the supercooled liquid, the coexistence line would terminate in a liquid-liquid critical point (LLCP). The hypothesis of a liquid-liquid coexistence with a second critical point in a region of metastability stimulated many studies involving experiments, theoretical approaches, and computer simulations; see Refs. 1 and 5–11. The region where the LLCP would be located is called no-man's land since it was considered unreachable because of the strong tendency of water to crystallization. Nonetheless recently new experimental techniques opened the possibility of exploring the no-man's land[12] and found new results corroborating the LLCP hypothesis.[2,13]

Different studies on supercooled water evidenced the relevant role in the phenomenology of the Widom line.[1,2,9] The Widom line is a general concept of critical phenomena and it is the locus of the maxima of the correlation length emerging upon approaching the critical point from the one phase region. The anomalous behavior can be interpreted by considering liquid water as a mixture of two distinct groups of molecules characterized by a different arrangement of the hydrogen bond (HB) network.[1,14–19] The LDL component, characterized locally by a stronger tetrahedral order, and the HDL component with a broken, more disordered, HB structure in analogy with the corresponding glassy states of the LDA ice and the HDA ice.[20–24] In this framework, the Widom line separates the region where the HDL component prevails from the one where the LDL component prevails.

Since the freezing point of water can be lowered by the addition of salt, the research on water in the supercooled region has recently increased the interest in the study of the behavior of salt solutions in that region.[10,25–27] Computer simulations[10,27] showed that the second critical point is present in salty water for low salt concentrations.

According to the Hofmeister classification scheme, anions and cations are ordered according to their properties of enhancing (structure makers) or weakening (structure breakers) the HB network of water. Structure makers will be strongly hydrated since they break the HB in the surrounding water molecules and the rest of the water molecules can rearrange in an ordered hydration structure. On the contrary, structure breaker ions interact weakly with the water and induce a disorder in the network of water.[28] Evidence from experiments

and computer simulations indicates that ions perturb the water structure beyond the first hydration shell with an effect similar to the application of pressure on pure water.[26,29,30] A new classification scheme recently emerged with the idea that different ions could modify the local balance between HDL and LDL components of water.[25]

Among the ionic aqueous solutions, lithium chloride solutions play an important role in this direction because of the ease in supercooling. Years ago, Moran[31] while studying the phase diagram of binary LiCl–$H_2O$ discovered a very relevant property of the aqueous lithium chloride solution, that is, its persistence in the liquid state over a large temperature drop.

Since that early times the metastable phase diagram of LiCl–$H_2O$ solutions has been studied.[31,32] Near the eutectic concentration, at $R \sim 6$, where $R$ is the water-salt molar mass ratio, the liquid can be supercooled directly to the glass transition, without thermal or kinetics phenomena that hamper it. Successive studies showed that this happens for concentrations that can be varied from $R = 4$ to $R = 7$ by changing the cooling rate of the solutions.[33]

The LiCl:6$H_2O$ is therefore a glass-forming liquid with a glass transition temperature $T_g = 135$ K, with the peculiarity that crystallization is avoided.

Here we study with molecular dynamics (MD) the dynamical and structural properties of LiCl:6$H_2O$ upon supercooling. We use a model potential that was recently introduced to study salt solutions.[34]

Our studies are motivated by the amount of experimental work performed on this solution. In particular, the dynamic structure factor of the supercooled solution has been wideband characterized by the joint analysis of photon correlation spectroscopy, Brillouin light scattering (BLS), inelastic uv scattering (IUVS), inelastic X-rays scattering (IXS) spectra. This investigation[35,36] has revealed the onset of the typical structural $\alpha$-relaxation of glassformers in the solution and the onset of a secondary Johari-Goldstein $\beta$-relaxation. Interestingly this latter onset upon cooling happens in coincidence with the temperature at which the properties of water seem to diverge and the $\alpha$-relaxation has a fragile character down to the glass transition.

In Sec. II, we describe the technical details of our simulations. In Sec. III, we present the results obtained in the study of the self-intermediate scattering function of water in the solution upon supercooling. In Sec. IV, we discuss the agreement with the Mode Coupling Theory, a theory that is able to take into account the dynamic behavior of glassformers in the region of mild supercooling.[37] In Sec. V, we start to describe the structural properties by considering the hydration properties of the ions. In Sec. VI, we perform a detailed analysis of the water structure in the solution in comparison with pure water. Section VII is devoted to conclusions.

## II. MODEL POTENTIAL AND SIMULATION DETAILS

In our simulation of the LiCl-water solutions, we use the JC-TIP4P/2005 site potential.[34] This potential is an improved version of the force field proposed by Joung and Cheatham (JC) for LiCl.[38] The JC-TIP4P/2005 potential has a better agreement with experiments, in particular, with the ion pairing radial distribution function. Besides this potential was specifically tested to work with TIP4P/2005 that we use in this work for water, while the original Joung and Cheatham potential was not.

In the JC-TIP4P/2005 force field each ion is a Lennard-Jones (LJ) site, the ions LJ parameters are those already introduced by Joung and Cheatham (JC),[38] the electrostatic charges are $+e$ for the $Li^+$ ion and $-e$ for the $Cl^-$ ion. The water is represented with the TIP4P/2005 potential.[39] This potential is one of the most used potentials for water as it reproduces very well several experimental features of water.[40] It is a four-site model, where the oxygen site is neutral, the hydrogen sites are positively charged, and a massless site shifted from the oxygen carries the negative charge. The oxygen sites interact with a LJ potential, while the charged sites interact only with the Coulombic forces.

The potential between the ions and the water sites can be written as a combination of a LJ and a Coulombic electrostatic potential in the form

$$u(r_{ij}) = 4\epsilon_{ij}\left[\left(\frac{\sigma_{ij}}{r_{ij}}\right)^{12} - \left(\frac{\sigma_{ij}}{r_{ij}}\right)^{6}\right] + \frac{q_i q_j}{4\pi\epsilon_0 r_{ij}}, \qquad (1)$$

where $r_{ij}$ is the distance between two interacting particles and $q_i$ is either the charge of an ion or the charge of a water site. In the potential between the ions, the crossed interactions are obtained by modifying the Lorentz-Berthelot (LB) combining rules,

$$\epsilon_{ij} = \chi \cdot \sqrt{\epsilon_{ii} \cdot \epsilon_{jj}}\,; \qquad \sigma_{ij} = \eta \cdot \frac{\sigma_{ii} + \sigma_{ij}}{2}, \qquad (2)$$

with $\chi = 1.88$ and $\eta = 0.934$. The modification of the LB rule has been introduced to obtain the ion pairing structure in agreement with experimental results.[34]

The JC-TIP4P/2005 ion-water and ion-ion parameters for the LJ form of the potential used in this work are reported in Table I.

All-atom MD simulations on the LiCl:6$H_2O$ system were performed at constant pressure $p = 1$ bar and temperatures spanning from $T = 300$ K down to $T = 200$ K. The cubic simulation box ($L = 2.61$ nm at $T = 300$ K) contains 480 water molecules, 80 $Cl^-$ ions, and 80 $Li^+$ ions. This gives a concentration of 14% corresponding to $c \approx 9.25$ mol/kg.

The cutoff radius for the non-bonded van der Waals interactions was set to 0.95 nm. The Coulombic interaction was also truncated at 0.95 nm, the correction contribution was evaluated by using the particle mesh Ewald method. The

TABLE I. Water-water, ion-water, and ion-ion LJ interaction parameters in the JC-TIP4P/2005 potential.[34]

| Atom pair | $\epsilon_{ij}$ (kJ/mol) | $\sigma_{ij}$ (nm) |
|---|---|---|
| O–O | 0.774 90 | 0.315 89 |
| $Li^+$–$Li^+$ | 0.435 09 | 0.143 97 |
| $Cl^-$–$Cl^-$ | 0.048 79 | 0.491 78 |
| $Li^+$–O | 0.580 65 | 0.229 93 |
| $Li^+$–$Cl^-$ | 0.273 92 | 0.296 26 |
| $Cl^-$–O | 0.194 44 | 0.403 83 |

TABLE II. Summary of the simulated state points at $p = 1$ bar including the temperature $T$, density $\rho$, and potential energy $U$ of the LiCl:6$H_2O$ system. At each temperature, the equilibration run of length $t_{eq}$ is followed by the data collection for a time $t_{prod}$.

| $T$ (K) | $\rho$ (g/cm$^3$) | U (kJ/mol) | $t_{eq}$ (ns) | $t_{prod}$ (ns) |
|---|---|---|---|---|
| 300 | 1.777 | −288 531 | 40 | 30 |
| 290 | 1.781 | −312 829 | 60 | 20 |
| 280 | 1.787 | −312 829 | 60 | 20 |
| 270 | 1.793 | −312 829 | 100 | 20 |
| 260 | 1.797 | −337 058 | 60 | 20 |
| 250 | 1.800 | −349 416 | 60 | 20 |
| 240 | 1.803 | −361 738 | 60 | 40 |
| 230 | 1.803 | −374 200 | 60 | 40 |
| 220 | 1.806 | −386 309 | 120 | 40 |
| 210 | 1.813 | −398 196 | 120 | 40 |
| 205 | 1.825 | −404 481 | 120 | 40 |
| 200 | 1.804 | −409 764 | 120 | 40 |

equations of motion are integrated with a time step of 1 fs with the Verlet leap-frog algorithm. Berendsen thermostats[41] were used to handle both the temperature and the pressure of the system. The MD simulations were performed using the parallelized version of the GROMACS 4.5.5[42] simulation package.

Table II shows the summary of the thermodynamic points investigated in this work. Details include the density of the system $\rho$, the potential energy $U$, and the simulation time for equilibration and production runs. Equilibration runs are longer than production runs to ensure, especially upon cooling, that the system of water and ions equilibrates properly at each temperature. The production run length is set to have enough statistics for the calculation of the static and dynamics density correlators. The total computational time amounts to about 1680 ns for the entire simulated isobar.

## III. DYNAMICS OF WATER IN THE SOLUTION UPON SUPERCOOLING

In the study of density fluctuations in a supercooled region, it was found years ago that the dynamics of water follow the Mode Coupling Theory (MCT).[43,44] MCT predicts that the dynamical relaxation of a density correlator upon supercooling shows three time regions. In the first ballistic region, the particle is not interacting with the others, and below a certain temperature it enters in the intermediate region, the so-called $\beta$-relaxation zone. The main feature of the $\beta$-relaxation is the presence of a plateau, the manifestation of the *cage* effect at the microscopic level. The particle is trapped in the cage formed by the nearest neighbors. The transient caging becomes longer and longer as supercooling progresses. When the cage relaxes, the particle can diffuse. This corresponds to the $\alpha$-relaxation characterized by a stretched exponential decay. The two-step relaxation after the ballistic decay is generally observed in glass formers upon cooling.

The $\alpha$ decay is determined by a relaxation time $\tau_\alpha$ that increases at decreasing temperature. MCT predicts that $\tau$ diverges with a power law

$$\tau_\alpha \sim (T - T_C)^{-\gamma} \tag{3}$$

in approaching the temperature $T_C$. In MCT, this divergence is interpreted as the sign of an ideal transition from an ergodic to a non-ergodic regime where the cages are frozen. At this level, MCT neglects hopping effects that in most glass formers intervene around $T_C$ to restore ergodicity and correspondingly modify the asymptotic behavior of $\tau_\alpha$.

In our supercooled solution, we consider the self-intermediate scattering function (SISF) of the oxygens calculated from our MD trajectories and defined as follows:

$$F^s_{OO}(q,t) = \frac{1}{N}\left\langle \sum_{i=1}^{N} e^{i\vec{q}\cdot[\vec{r}_i(t)-\vec{r}_i(0)]} \right\rangle, \tag{4}$$

where $N$ is the number of water molecules, $\vec{r}_i(t)$ is the position of the oxygen atom of the i-th water molecule at time $t$, and $\vec{q}$ is the wavevector (transferred in an experiment). This quantity is the spatial Fourier transform of the single particle density-density correlator. We perform the calculations at the wavevector corresponding to the position of the peak of the oxygen–oxygen structure factor of water $q_0 = 2.25$ Å$^{-1}$, that is, the wavevector at which the MCT features are best evident (see Sec. IV).

The results are shown in Fig. 1 for all the twelve simulated temperatures that span from $T = 300$ K down to $T = 200$ K.

Already at $T = 300$ K, a plateau starts to appear after the ballistic transient. This behavior can be explained in the framework of MCT as stated above.

The SISF of water in solution has a behavior similar to bulk water; the presence of the plateau already at ambient temperature, however, indicates that the dynamics of water with LiCl is slower with respect to bulk water where the plateau develops later.[45,46] Just below $T = 300$ K, the two-step relaxation is already clearly visible and there is clear evidence of the slow $\alpha$-relaxation. The overshoot feature observed for temperatures lower than 250 K is called the boson peak and it is also a feature typical of glass formers.[47]

The overall curves can be fitted with the formula used also for bulk water,[43,44]

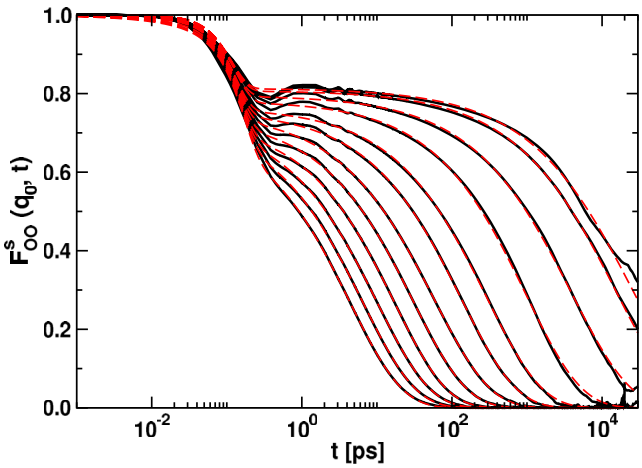


FIG. 1. Oxygen–oxygen SISF in LiCl:6$H_2O$ calculated at $q_0 = 2.25$ Å$^{-1}$, the position of the first peak of the oxygen structure factor. The bottom curve corresponds to the temperature $T = 300$ K; the top curve corresponds to $T = 200$ K. The continuous curves are results from the simulations, while the dashed curves are the fit to Eq. (5).

$$F_s(q,t) = [1 - f_q]e^{-(t/\tau_s)^2} + f_q e^{-(t/\tau_\alpha)^\beta}, \quad (5)$$

where $f_q$ is the Lamb-Mössbauer factor, $\tau_s$ is the characteristic time of the initial fast relaxation, $\tau_\alpha$ is the $\alpha$-relaxation time, and $\beta$ is the Kohlrausch exponent. The best fitting curve at each temperature is shown superimposed to the data point in Fig. 1. The parameters extracted from the fitting procedure are shown in Fig. 2.

In the top panel of Fig. 2, the characteristic time $\tau_s$ is plotted as a function of temperature. It is of order 0.15 ps, and it has a weak temperature dependence as expected in the ballistic regime.

The Lamb-Mössbauer factor, $f_q$, which arises from the cage effect, is plotted in the middle panel of the same figure. It increases upon cooling reflecting the decrease of the characteristic distance over which the particle rattles inside the cage due to the interactions with the first nearest neighbor molecules. Through the relation $f_q = e^{-a^2q^2/3}$, we can estimate the scale length $a$ of this motion, the cage radius. It comes out $a = 0.43$ Å at $T = 300$ K and $a = 0.35$ Å at $T = 200$ K. As expected both these radii are shorter than the first nearest neighbors' distance as evidenced from the radial distribution functions shown in Sec. VI. The shortening of the cage radius upon decreasing temperature is related to the decrease of $\tau_s$. Finally, in the same figure, the stretching parameter of the $\alpha$-relaxation, $\beta$, is reported. It is rather constant in temperature from $T = 300$ K down to $T = 220$ K, and it decreases slightly below this temperature. Also this decreasing trend is typical in glass forming materials. To compare with simulations of bulk water along the 1 bar isobar, $\beta$ of SPC/E water varies within the interval 0.9-0.6 upon cooling, and the same occurs in the TIP4P and TIP4P/2005 water potential along the 1 g/cm$^3$ isochores.[45,48] Our $\beta$ values reveal therefore that the dynamics of water is more stretched in LiCl:6H$_2$O than in bulk water spanning from circa 0.63 to 0.53 for the temperatures that we investigated.

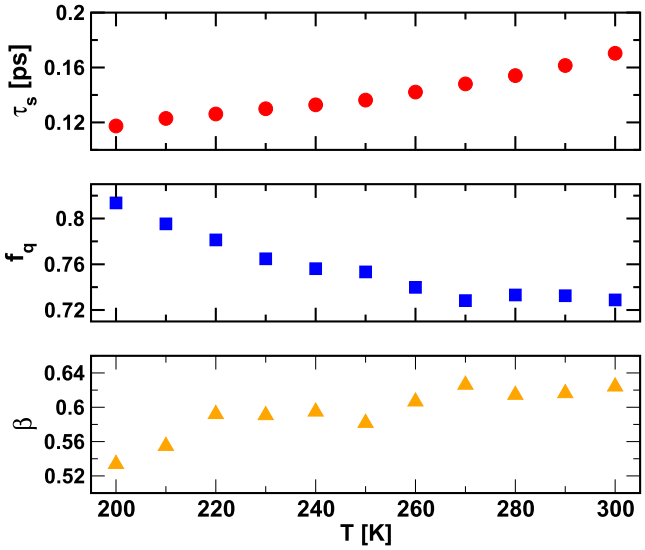


FIG. 2. Fast-relaxation times $\tau_s$, Lamb-Mössbauer factors $f_q$, and stretching parameters of the $\alpha$-relaxation, $\beta$, extracted from the fit procedure via Eq. (5) of the oxygen-oxygen SISF in LiCl:6H$_2$O. Data are shown as a function of the temperature of the system.

## IV. $\alpha$-RELAXATION AND MCT

As said above, the other relevant quantity that characterizes the dynamics of supercooled water is the structural $\alpha$-relaxation time, $\tau_\alpha$. This quantity, as extracted from the fit of our SISFs, is plotted in the log-lin plot in Fig. 3 as a function of temperature. The $\alpha$-relaxation in LiCl:6H$_2$O is clearly slower than in bulk water. Typically, $\tau_\alpha$ in bulk water varies from 1 to 1000 ps upon cooling the system in the range 300–200 K. It is common in the literature to describe the temperature behavior of the relaxation time of glass-forming liquids with the phenomenological Vogel-Fulcher-Tammann (VFT) law, given by

$$\tau_\alpha = \tau_0 \exp\left[\frac{BT_0}{T - T_0}\right], \quad (6)$$

where $\tau_0$, $B$, and $T_0$ are constants. $T_0$ is a point of singularity of $\tau_\alpha$, and it can be interpreted in terms of the Adam and Gibbs theoretical approach to the glass transition,[49] but its relation with the real glass transition temperature is highly debated.[5] $B$ is the fragility parameter whose variations between 5 and 100 can describe supercooled liquids from fragile to strong extremes in the Angell plot.[50]

The relaxation times of water in LiCl:6H$_2$O are found to obey the VFT law, reported in Fig. 3, which well describes the temperature behavior of $\tau_\alpha$ in the entire regime of temperature spanned by our simulation. We found $B = 7.56$, which classified the water of our solution as a fragile liquid and $T_0 = 132.3$ K, which is close to the values found from VFT fitting to experimental results 148 ± 16 K on LiCl:7.3H$_2$O.[51]

Finally, we can also estimate the glass transition temperature of the solution with our model. From the VFT equation, since conventionally $\tau_\alpha(T_g) = 100$ s, extrapolating that value of $\tau_\alpha$ we found $T_g = 159.5$ K.

In computer simulation of TIP4P/2005 bulk water, it has been found that in the mild supercooled region the dynamics of water can be described in terms of MCT.[45] In Fig. 3, we show that in our LiCl solution the temperature dependence of

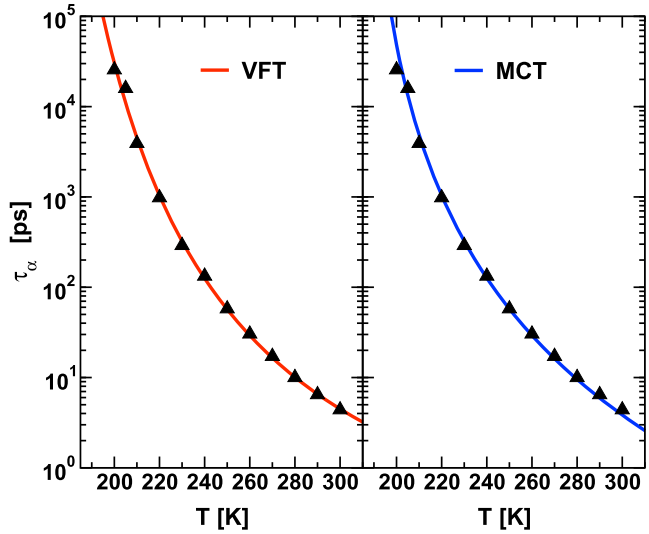


FIG. 3. Structural $\alpha$-relaxation time of water in LiCl:6H$_2$O as a function of temperature. Data are extracted from the fit procedure via Eq. (5) of the oxygen-oxygen SISF. The Vogel-Fulcher-Tammann approximation and the MCT fit with Eq. (3) are also shown superimposed to the data points.

the $\tau_\alpha$ also follows the power law prediction of the MCT of Eq. (3).

The best fit is obtained by excluding the two lowest temperature points. Nonetheless also at low temperature, the agreement with the MCT law is rather good. This can be also appreciated in Fig. 4, where the structural $\alpha$-relaxation time and its MCT power law fit are shown as a function of inverse temperature in an Arrhenius plot on the left panel and as a function of the distance from the MCT temperature on the right panel.

The extracted parameters are $\gamma = 4.60$ and $T_C = 185.0$ K. The value of $\gamma$ is rather high with respect to the bulk. For the sake of comparison, $\gamma \sim 3$ in TIP4P/2005 water, along isochores in the range $\rho = 0.95$–$1.03$ g/cm$^3$.[45] Also in the simulation of NaCl aqueous solution at very diluted condition, the $\gamma$ exponent is different from its bulk value.[52] Concerning the MCT temperature, it has been shown[37] that for fragile liquid $\frac{T_C}{T_g} \leq 1.2$. For our results, we estimated $\frac{T_C}{T_g} \simeq 1.15$, which gives further support to the fact that the MCT temperature found is compatible with a fragile behavior of the glass-former. Globally the MCT power law describes well the structural relaxation times of the water in LiCl:6H$_2$O in a temperature region starting from $T = 300$ K down to the mild supercooled region. Upon further cooling the system, a slight deviation from the MCT power law is found for the very lowest temperatures that we could reach with simulation starting from ~205 K.

In the deep supercooled region of bulk TIP4P/2005 water a deviation from the MCT (fragile) behavior is observed with a crossover from a fragile to a strong Arrhenius behavior.[45] A fragile to strong crossover (FSC) was found in other simulations of bulk water[9,48] and in NaCl aqueous solution with a concentration of 0.67 mol/kg.[52] The phenomenon is driven by hopping effects neglected in MCT.[46] In supercooled water, this crossover takes place in the single phase region above the LLCP at the crossing of the Widom line. The system crosses from a region where the HDL component (fragile) prevails to a region where the LDL component (strong) prevails.[1] In our LiCl solution, the FSC was not found, so either it is not present or it could be shifted below 200 K.

It must be noted that the $\alpha$-relaxation of LiCl–6H$_2$O found in our simulation is in agreement with experiments. From high temperature, it obeys to the power scaling law similar to MCT prediction down to T ~ 200.[53] Similar behavior is also found for the viscosity of the eutectic liquid:[54] the viscosity data are consistent with the MCT power law, while the VFT law describes the temperature behavior over the entire temperature range investigated in that work (down to 180 K).

## V. HYDRATION OF IONS AND IONS' CORRELATION

We now analyze the structural properties of our aqueous solution by calculating the radial distribution function (RDF). In Fig. 5, the correlations between the water oxygen atom and the two ions, $g_{OX}(r)$ where X = Li, Cl, are compared at two selected temperatures, $T = 300$ K and $T = 200$ K.

OX correlations exhibit no appreciable differences upon cooling, apart from the general sharpening of peaks.

In the case of lithium, a well-defined shell of lithium atoms is formed around the oxygen, as seen from the intense first peak located at 0.19 nm followed by a deep first minimum. The first shell of chlorine atoms around the oxygen is centered at 0.32 nm and it is less sharply defined with respect to the lithium first shell, as indicated by the shoulder already present at ambient temperature and the less deep first minimum. The positions of the peaks are unchanged at the two temperatures. From this comparison, it can be also appreciated that chlorine coordination shells lie between lithium coordination shells, and this implies an alternation of charges indicating charge ordering around the oxygen atoms. We also note that the first peak of the $g_{OCl}(r)$ falls at a distance of 0.32 nm which is very close to the $g_{OO}(r)$ first peak, 0.28 nm. This shows that the Cl has a tendency to replace the oxygen in the water network. This feature has been also found in simulations of water and $Na^+$ $Cl^-$ both in the liquid[26] and in the crystal phase where a crystal slab grown from a coexisting aqueous solution shows that the $Cl^-$ always goes substitutional to the oxygen in the doped ice and that the $Na^+$ is always included as an interstitial defect.[55]

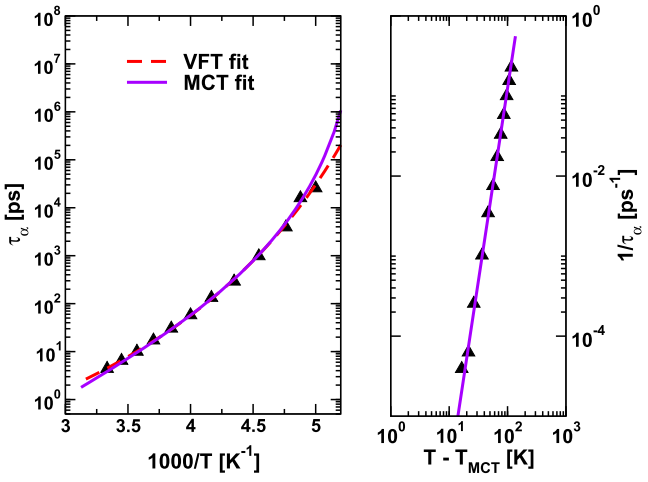


FIG. 4. Structural $\alpha$-relaxation time of water in LiCl:6H$_2$O. Left panel: $\tau_\alpha$ as a function of the inverse temperature. Data (triangle up) are fitted with MCT, $T_{MCT} = 183.58$ K (continuous line), and VFT, $T_0 = 132.3$ K (broken line). Right panel: log-log plot of $1/\tau_\alpha$ vs. $T - T_C$. The MCT fit is also shown as the continuous line superimposed to the data points.

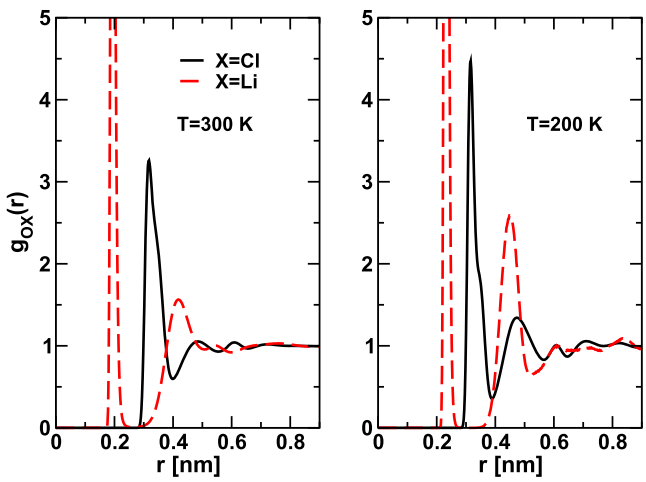


FIG. 5. Oxygen-chlorine RDFs and oxygen-lithium RDFs in LiCl:6H$_2$O for the two indicated temperatures.

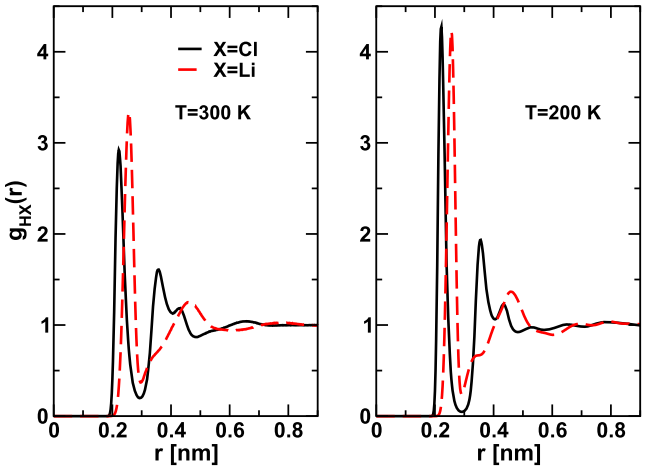


FIG. 6. Hydrogen-chlorine RDFs and hydrogen-lithium RDFs in LiCl:6$H_2O$ at the indicated temperatures.

Figure 6 is the analogous of Fig. 5 for the hydrogen-ions' correlations, $g_{HX}(r)$, X = Li, Cl. Also in this case, the decrease of temperature does not produce appreciable changes in the RDFs, and the positions of the principal peaks are in fact unchanged. The first peaks of the H–Cl RDF lie at = 0.22, 0.36, and 0.39 nm. The coordination shells of lithium shift to longer distances with respect to chlorine, they are located at 0.26 nm and 0.47 nm, and a shoulder on the left of the second peak is observed at 0.34 nm.

From the figures, it is clear that the position of the first peak of the $g_{LiH}$ is shifted to a higher distance with respect to the position of the first peak of the $g_{LiO}$ and that the opposite is true for $g_{ClH}$ and $g_{ClO}$. This is the consequence of the electrostatic interactions between the polar water molecule and the charged ions, with water molecules that arrange in such a way that the oxygen is exposed to the positive charged ion, $Li^+$, and the hydrogen atoms oriented to the negative charged ion, $Cl^-$.

In Fig. 7, we report the coordination numbers of water oxygens and hydrogens around the two ions $Li^+$ and $Cl^-$. We see that the coordination number of each couple does not change much with temperature and does not show any trend.

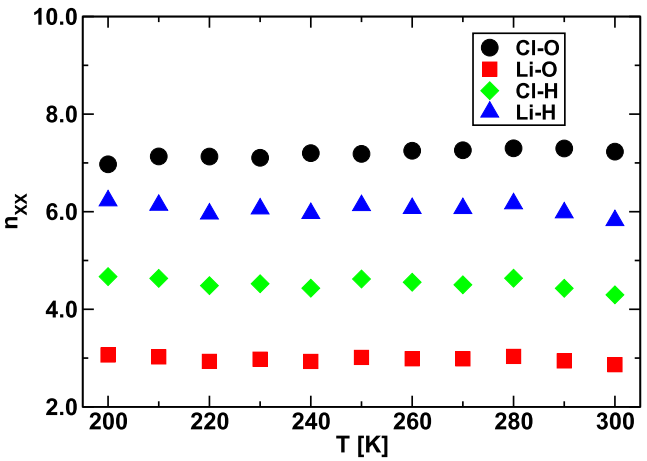


FIG. 7. Coordination number of oxygens and hydrogens around lithium and chlorine as a function of temperature.

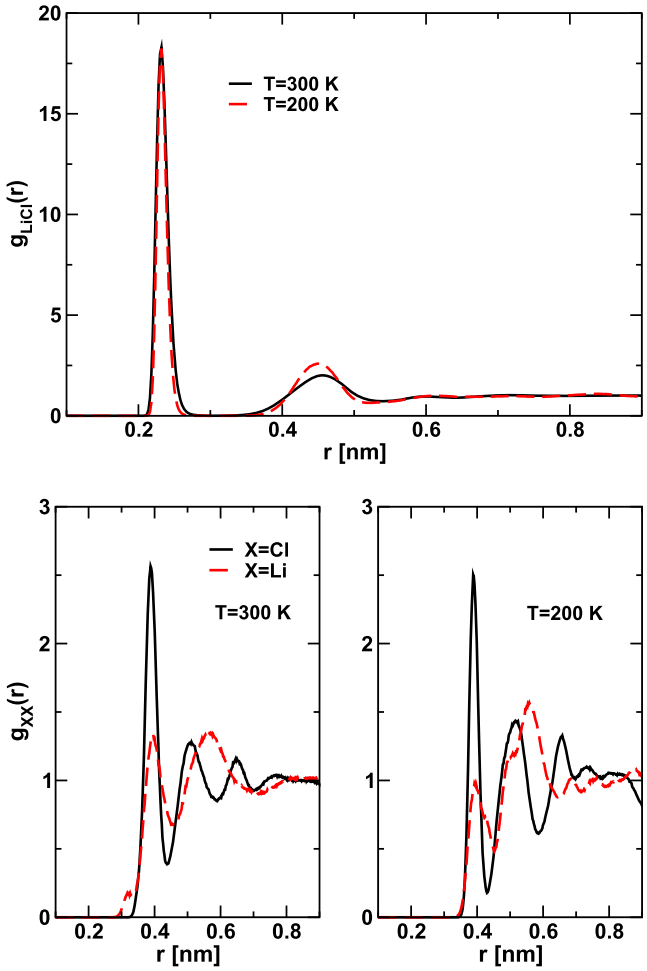


FIG. 8. Ion-ion RDF in LiCl:6$H_2O$ at $T$ = 300 K and $T$ = 200 K. In the top panel, lithium-chlorine RDFs; in the bottom panels, lithium-lithium (black line) and chlorine-chlorine (red line) RDFs at the indicated temperatures.

In Fig. 8, the RDFs that characterize the ion-ion structure are shown. In the top panel, $g_{LiCl}(r)$ is shown at two selected temperatures, T = 300 K and T = 200 K. Both the curves show a much intense first maximum at 0.23 nm and a second peak at 0.45 nm. The separation between these two peaks reveals the presence of a water molecule included between the two ions. In the bottom panels, Li–Li and Cl–Cl RDFs are reported. The Li-Li RDF shows at $T$ = 300 K a broad peak at 0.56 nm also observed experimentally, and a well-defined pre-peak at 0.396 nm has been observed in hyperquenched samples (for the discussion of this peak, see Ref. 34). At low temperature, the position of this pre-peak is unchanged, while the second shell is modulated in a double peak structure. At long distance, other peaks are observed. $g_{ClCl}(r)$ appears more structured with respect to $g_{LiLi}(r)$, showing a second shell and a third shell sharply defined at both high and low temperatures. The diversification on the long range order between the two ions can be due to their different sizes. Finally, the structure of ions seems to be more temperature dependent, especially for the long distance behavior of the RDF. We collect in Table III the positions of different peaks, and we include also the oxygen and hydrogen positions of water in solution that we describe in Sec. VI.

TABLE III. Intermolecular peak positions extracted by the correlations of the LiCl:6$H_2O$ system. Between parentheses is the value of Ref. 56. The value of water structure is also reported.

| Type | 1st (nm) | 2nd (nm) | 3rd (nm) |
|---|---|---|---|
| O–O | 0.28 (0.29)[a] | 0.43 (0.44) | |
| O–H | 0.18 (0.188)[a] | 0.32 (0.337) | 0.38 |
| H–H | 0.23 (0.24) | 0.37 (0.37) | 0.41 |
| Li–Cl | 0.23 | 0.45 | ... |
| Li–O | 0.19 (0.2) | 0.43 | |
| Li–H | 0.26 | 0.47 | |
| Li–Li | 0.4 | 0.56(+prepeak) | |
| Cl–O | 0.316 (0.3175)[a] | 0.47 | |
| Cl–H | 0.22 (0.2225) | 0.36 (0.3625) | 0.39 |
| Cl–Cl | 0.39 | 0.51/2 | 0.65/6 |

[a]Glass from Ref. 56.

Concerning the experimental values, reported in parentheses, in Table III, those values compete to two state points: the supercooled LiCl:6$H_2O$ at $T$ = 162 K, and the glassy LiCl:6$H_2O$ at $T$ = 120 K, derived from neutron pair correlation functions investigated by Prevel *et al.*[56]

We report these values when no available data for the supercooled liquids are found because Prevel *et al.*[56] have found that no significant changes appear in the glassy state with respect to the (deep) supercooling liquids' RDFs. We see that most of the positions that we derived at much higher temperature are in very good agreement with the experimental values of both the liquids and the glass. This shows that the JC-TIP4P/2005 model describes well the molecular interactions of LiCl:6$H_2O$, also at low temperature.

## VI. WATER CORRELATIONS

### A. Water structure

To see the effect of ions on the water structure, we compare the RDFs calculated for water in LiCl:6$H_2O$ with the respective functions of bulk TIP4P/2005 water at ambient pressure. We consider the three intermolecular RDFs $g_{ij}(r)$, where $i, j$ are the oxygen and hydrogen atoms ($i, j$ = O, H) and the atom pairs $i, j$ do not belong to the same molecule.

We present the $g_{OO}(r)$ in Fig. 9, the $g_{OH}(r)$ in Fig. 10, and the $g_{HH}(r)$ in Fig. 11. The RDFs are shown at the highest, $T$ = 300 K, and at the lowest, $T$ = 200 K, simulated temperatures.

From the comparison between the RDFs of bulk water and the RDFs of water in solution, we can see that LiCl has a strong effect on the structure of water.

The positions of the first sharp intermolecular peaks of OO, OH, and HH correlations are reported in Table III. At $T$ = 300 K, the effect of the salt on the $g_{OO}(r)$ appears to be relevant. The position of the first peak is unaffected, but it is lower and broader in the solution. The first minimum is shifted to a higher distance, and it is less well-defined in solution; as a consequence the first shell at room temperature appears less rigid with a broadening due to the increase of penetration from the second to the first shell. At the lowest temperature, the first shell partially shrinks and the broadening of peak degenerates into a shoulder at 0.32 nm. The broadening of the first peak and the modifications around the first minimum are the signature of the distortion of the short range order of oxygen atoms due to the interactions with ions. The distortion effect appears stronger at the lowest temperature.

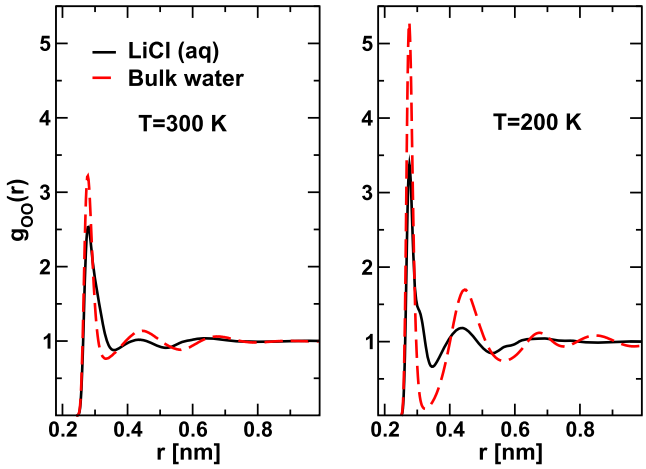


FIG. 9. Oxygen-oxygen RDFs in LiCl:6$H_2O$ (full black line) compared with the pure water (broken red line) at the two indicated temperatures $T$ = 300 K and $T$ = 200 K.

We note that the first peak of the OH RDF representing the hydrogen bond at about 0.19 nm is almost unchanged in position with a small reduction of the maximum. We also note in the solution some changes in the second shell, more evident for lower temperatures. Also the HH RDF, which represents the orientational correlation between neighboring pure water molecules, behaves similarly to the OH RDF in the aqueous solutions, namely, the first peak is less sharp in the solution and the successive shells show some difference with respect to bulk. These results reveal the preservation of the hydrogen bonds between water molecules in the system.

Importantly we note that decreasing the temperature has a mild effect on the maxima and minima of the $g_{ij}(r)$ in solution, while the effect is very strong in bulk water.

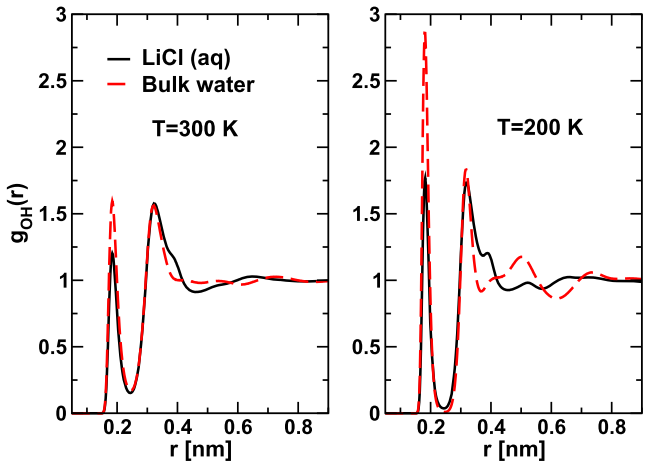


FIG. 10. Oxygen-hydrogen RDFs in LiCl:6$H_2O$ (full black line) compared with the pure water (broken red line) at the two indicated temperatures $T$ = 300 K and $T$ = 200 K.

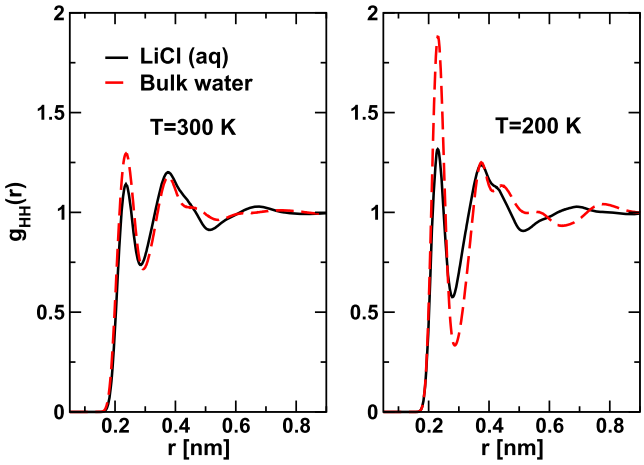


FIG. 11. Hydrogen-hydrogen RDFs in LiCl:6$H_2O$ (full black line) compared with the pure water (broken red line) at the two indicated temperatures $T$ = 300 K and $T$ = 200 K.

While the hydrogen bonds are preserved, the changes in the OO correlation indicate a distortion of the HB network. The modification of the second shell of the oxygens has been already observed in other ionic solutions, and it indicates that the presence of the ions acts as an increase of pressure on water.[26] The collapse of the second hydration shell is directly associated with the angular perturbation of the water tetrahedral network, and we will give in Subsection VI B further evidence of this point.

In recent experimental and computer simulations on water, it was found evident that the relative importance of LDL and HDL forms of water can be determined from an analysis of the $g_{OO}(r)$ in the intermediate range beyond the third peak, and this analysis is connected to the local structure index (LSI) of Shiratani-Sisai[57,58] already applied to supercooled water.[59–61] In particular, it was found that the fourth OO peak of pure water was shifted to longer distances as the HDL component prevails.[62]

In Fig. 12, we report the OO RDF magnified by plotting the quantity $4\pi r^2(g_{OO}(r) - 1)$ in the range that we

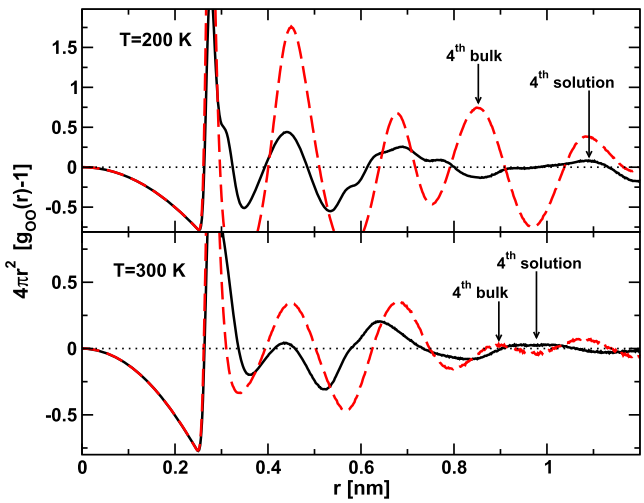


FIG. 12. Oxygen-oxygen RDFs in LiCl:6$H_2O$ (full black line) compared with the pure water (broken red line) reported as $4\pi r^2\ [g_{OO}(r) - 1]$ to magnify the intermediate range. In the bottom panel, $T$ = 300 K; in the top panel, $T$ = 200 K.

can explore in our simulation compared with bulk water. At $T$ = 300 K, there is evidence that the fourth OO peak is shifted to a higher distance in LiCl:6$H_2O$ with respect to bulk water. This can be interpreted as evidence of an increase of the HDL component in water due to the presence of the ions.

At $T$ = 200 K, we note that in pure water the fourth peak of the $g_{OO}(r)$ shifts slightly to lower distances with respect to the peak at $T$ = 300 K, and this indicates that at decreasing temperature in TIP4P/2005 the LDL component increases. Instead the $g_{OO}(r)$ of the solution shows broadening in the intermediate range where it is evident a further shift of the fourth peak to a higher distance.

## B. Hydrogen bond network

The water radial distribution functions reveal distortion of the hydrogen bond network in our solution with an increase of the HDL component. This motivated the calculation of the angular distribution of water, $P(\gamma)$, in LiCl:6$H_2O$ solution. The angle $\gamma$ is defined as the angle between the two vectors joining the oxygen atom of a water molecule with the oxygen atoms of the two closest water neighbors. The distribution of the values of $\gamma$ angles assumed by water molecules characterizes the short range order present in bulk liquid water. Therefore it is possible to monitor perturbation on the water hydrogen bond network due to the addiction of ions, by looking at this quantity.

The resulting water angular distribution $P(\cos\gamma)$ in LiCl:6$H_2O$ is shown in Fig. 13 compared with the distribution for pure water at 300 K. The curve for pure water shows, as usual, a main peak at around 103°, which is the signature of the tetrahedral order present in liquid water, and a secondary peak due to interstitial water molecules at around 53°. In LiCl:6$H_2O$, there is still a peak close to 103°, but the main

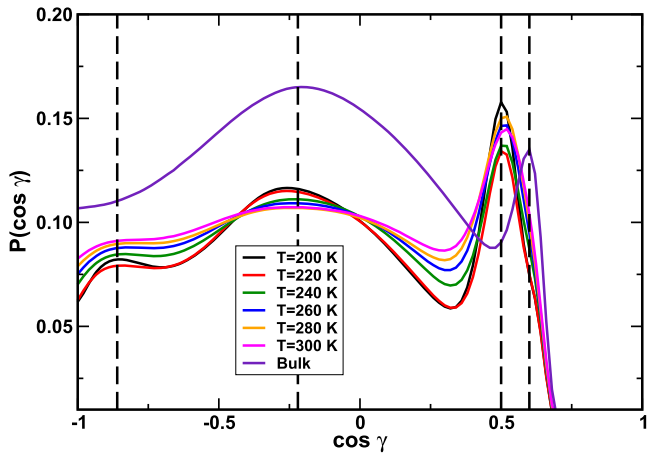


FIG. 13. Normalized angular distribution function $P(\cos\gamma)$ of the angle between the oxygens of three nearest neighbor water molecules. For water contained in the LiCl:6$H_2O$ solution, curves are shown from the highest simulated temperature $T$ = 300 K down to the lowest temperature $T$ = 200 K. It is also shown that the curve for bulk water at $T$ = 300 K shifted up to make more clear the comparison. The dashed vertical lines mark the positions of the peaks of the distributions. For pure water the peak at $\gamma$ = 103° approximates the pure tetrahedral order, while the peak at $\gamma$ = 53° is due to the interstitial molecules. For the solution, the main peak is located around $\gamma$ = 60° and there is a new peak at $\gamma$ = 150°.

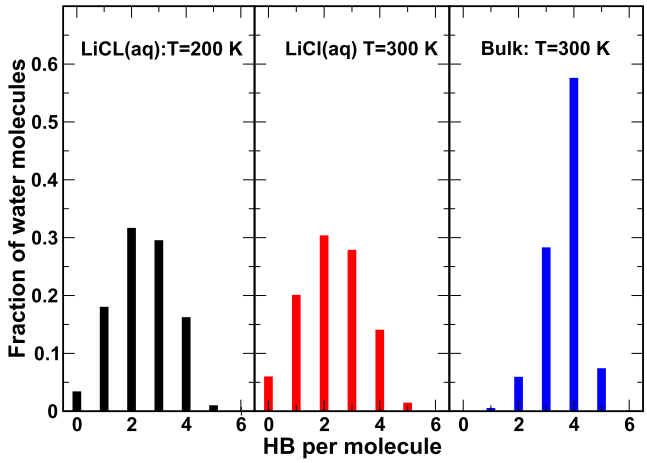


FIG. 14. Distributions of the number of hydrogen bonds per water molecule contained in the LiCl:6$H_2O$ solution for $T$ = 300 K and $T$ = 200 K compared with the distribution of bulk water.

peak is now located for all the temperatures at around 60°, indicating the large increase of the interstitial molecules. A third peak, missing in bulk water, is present, it sharpens toward low temperature, and it is located at ∼150°.

Although the tetrahedral peak of the angular distribution is not totally depressed indicating the presence of the bulk-like hydrogen bonds in the system, the distribution shows an increase of the interstitial molecules and the onset of a population of water molecules that assume a high $\gamma$ angle value. So we find another piece of evidence that the HB network in the solution is strongly distorted with respect to the network of bulk water.

Finally, the distribution of hydrogen bonds in the system has been calculated. We adopted the usual geometrical criterion for the definition of a hydrogen bond between two water molecules, i.e., the O–O distance less that 0.35 nm and the H–O$\cdots$O angle less than or equal to 30°.

In Fig. 14 we show the distributions of the number of hydrogen bonds per water molecule in the solution at two temperatures, $T$ = 300 K and $T$ = 200 K, compared with the distribution of pure water at $T$ = 300 K. This distribution in bulk water typically shows its maximum at $n$ = 4, as shown in the figure at $T$ = 300 K, and other values of $n$ are strongly depressed in bulk water upon cooling. In the case of the water in LiCl:6$H_2O$, most of the water molecules are involved in the formation of 2 or 3 hydrogen bonds. We can infer that the presence of a small number of molecules with four HBs in the solution is plausibly related to a large fraction of water molecules in an interstitial position or at a high angle in such a way that the geometrical constraints cannot be satisfied any more. In connection to this, we remark also the appearance of a non-zero population of water with no HB at all.

## VII. CONCLUSIONS

We performed MD computer simulations of the glass forming solution LiCl:6$H_2O$, under ambient pressure $p$ = 1 bar for temperature ranging in the interval 300–200 K. The potential used for describing the intermolecular interactions of atoms and molecules contained in the solution is the JC-TIP4P/2005,[34] in which water is described with the four-site TIP4P/2005 potential, while in the ion-ion interaction modified Lorentz-Berthelot mixing rules were implemented to better reproduce experimental properties of the system at ambient condition. The JC-TIP4P/2005 is found to perform well also at low temperature in reproducing the structure of the supercooled LiCl:6$H_2O$ solution.

We have calculated at decreasing temperatures from $T$ = 300 K to $T$ = 200 K the oxygen-oxygen SISFs to extract the dynamical properties upon supercooling of the water contained in the solutions, and we have also calculated the structural properties that characterize the hydration of the ions and the hydrogen bond network of water in solution.

The dynamics of water in the LiCl:6$H_2O$ solution are strongly slowed down by the interaction with ions, and the time scale of the $\alpha$-relaxation is a factor of 10 longer with respect to bulk supercooled water. Water in solution is also found to behave as a fragile liquid upon supercooling, which is in accordance with experimental determination. We found that MCT describes well the phenomenology in terms of the cage effect at all the investigated temperatures. The $\alpha$-relaxation time is found to follow the power law predicted by MCT, though a slight deviation appears at $T$ = 200 K. Only further extended simulations well below 200 K could clarify whether this is the signature of the onset of a dynamic crossover connected to the Widom line.

Concerning the structural properties, in analogy with other ionic aqueous solutions, the LiCl salt, while preserving the water hydrogen bond in the system, strongly affects the OO coordination shells of water. In particular, the modification of the second shell of the OO radial distribution function indicates a strong distortion of the tetrahedral water network. This has also been confirmed by the direct calculation of the angular distribution of three nearest neighbor molecules. The percentage of interstitial molecules increases a lot with respect to pure water, and a certain number of water molecules are found at an angle greater than the typical value characterizing the tetrahedral order of bulk water. Importantly decreasing the temperature has little effect on the maxima and minima of the $g_{ij}(r)$ in solution, while the effect is very evident in bulk water.

The changes introduced by the ions in the structure of water indicate that LiCl has the role of enhancing the HDL component. This is confirmed by looking at the details of the $g_{OO}(r)$ at intermediate distances. There is evidence that the $Li^+$ ion has the most relevant effect on water in comparison with $Cl^-$.[25] $Li^+$ is traditionally classified as a structure maker, but according to our results at this concentration $Li^+$ increases the HDL component in the two-state water. This is in agreement with recent experiments.[25] On the other hand at low salt concentration of LiCl, the oxygen-oxygen structure appears less distorted with respect to bulk water.[34] This indicates that the role of *structure maker/breaker* could depend on the concentration.

In computer simulations of NaCl(aq), it was found that increasing the salt concentration up to 2.10 mol/kg makes more stable the HDL phase shifting to higher temperature and more negative pressure the LLCP.[27] In the case we studied in the present work, the salt at the concentration of 9.25 mol/kg enhances the HDL component of water in such a way that it

prevents the possibility of a crossover from a fragile (more HDL) to a strong (more LDL) dynamical behavior. We can infer that this has the consequence that this solution is easy to supercool and to drive in the glassy state.


[1] P. Gallo, K. Amann-Winkel, C. A. Angell, M. A. Anisimov, F. Caupin, C. Chakravarty, E. Lascaris, T. Loerting, A. Z. Panagiotopoulos, J. Russo, J. A. Sellberg, H. E. Stanley, H. Tanaka, C. Vega, L. Xu, and L. G. M. Pettersson, Chem. Rev. **116**, 7463 (2016).
[2] P. Gallo and H. E. Stanley, Science **358**, 1543 (2017).
[3] R. J. Speedy, J. Chem. Phys. **86**, 982 (1982).
[4] P. H. Poole, F. Sciortino, U. Essmann, and H. E. Stanley, Nature **360**, 324 (1992).
[5] P. G. Debenedetti, J. Phys.: Condens. Matter **15**, R1669 (2003).
[6] S. Harrington, P. H. Poole, F. Sciortino, and H. E. Stanley, J. Chem. Phys. **107**, 7443 (1997).
[7] M. Yamada, S. Mossa, H. Stanley, and F. Sciortino, Phys. Rev. Lett. **88**, 195701 (2002).
[8] P. H. Poole, I. Saika-Voivod, and F. Sciortino, J. Phys.: Condens. Matter **17**, L431 (2005).
[9] L. Xu, P. Kumar, S. V. Buldyrev, S. H. Chen, P. H. Poole, F. Sciortino, and H. E. Stanley, Proc. Natl. Acad. Sci. U. S. A. **102**, 16558 (2005).
[10] D. Corradini, M. Rovere, and P. Gallo, J. Chem. Phys. **132**, 134508 (2010).
[11] J. L. F. Abascal and C. Vega, J. Chem. Phys. **133**, 234502 (2010).
[12] J. A. Sellberg, C. Huang, T. A. McQueen, N. D. Loh, H. Laksmono, D. Schlesinger, R. G. Sierra, D. Nordlund, C. Y. Hampton, D. Starodub, D. P. DePonte, M. Beye, C. Chen, A. V. Martin, A. Barty, K. T. Wikfeldt, T. M. Weiss, C. Caronna, J. Feldkamp, L. B. Skinner, M. M. Seibert, M. Messerschmidt, G. J. Williams, S. Boutet, L. G. M. Pettersson, M. J. Bogan, and A. Nilsson, Nature **510**, 381 (2014).
[13] K. H. Kim, A. Späh, H. Pathak, F. Perakis, D. Mariedahl, K. Amann-Winkel, J. A. Sellberg, J. H. Lee, S. Kim, J. Park, K. H. Nam, T. Katayama, and A. Nilsson, Science **358**, 1589 (2017).
[14] C. Huang, K. T. Wikfeldt, T. Tokushima, D. Nordlund, Y. Harada, U. Bergmann, M. Niebuhr, T. M. Weiss, Y. Horikawa, M. Leetmaa, M. P. Ljungberg, O. Takahashi, A. Lenz, L. Ojamae, A. P. Lyubartsev, S. Shin, L. G. M. Pettersson, and A. Nilsson, Proc. Natl. Acad. Sci. U. S. A. **106**, 15214 (2009).
[15] A. Nilsson and L. G. M. Pettersson, Chem. Phys. **389**, 1 (2011).
[16] V. Holten and M. Anisimov, Sci. Rep. **2**, 713 (2012).
[17] H. Tanaka, Phys. Rev. Lett. **80**, 5750 (1998).
[18] H. Tanaka, Eur. Phys. J. E **35**, 113 (2012).
[19] V. Holten, J. C. Palmer, P. H. Poole, P. G. Debenedetti, and M. A. Anisimov, J. Chem. Phys. **140**, 104502 (2014).
[20] O. Mishima, L. D. Calvert, and E. Whalley, Nature **314**, 76 (1985).
[21] K. Winkel, M. Elsaesser, E. Mayer, and T. Loerting, J. Chem. Phys. **128**, 044510 (2008).
[22] C. U. Kim, B. Barstow, M. V. Tate, and S. M. Gruner, Proc. Natl. Acad. Sci. U. S. A. **106**, 4596 (2009).
[23] K. Winkel, E. Mayer, and T. Loerting, J. Phys. Chem. B **115**, 14141 (2011).
[24] A. Nilsson and L. G. M. Pettersson, Nat. Commun. **6**, 8998 (2015).
[25] I. Waluyo, D. Nordlund, U. Bergmann, D. Schlesinger, L. G. M. Pettersson, and A. Nilsson, J. Chem. Phys. **140**, 244506 (2014).
[26] P. Gallo, D. Corradini, and M. Rovere, Phys. Chem. Chem. Phys. **13**, 19814 (2011).
[27] D. Corradini and P. Gallo, J. Phys. Chem. B **115**, 14161 (2011).
[28] B. Hribar, N. T. Southall, V. Vlachy, and K. A. Dill, J. Am. Chem. Soc. **124**, 12302 (2002).
[29] A. K. Soper and K. Weckström, Biophys. Chem. **124**, 180 (2006).
[30] R. Leberman and A. K. Soper, Nature **378**, 364 (1995).
[31] H. E. Moran, J. Phys. Chem. **60**, 1666 (1956).
[32] A. Elarby-Aouizerat, J. F. Jal, P. Chieux, J. M. Letoff, P. Claudy, and J. Dupuy, J. Non-Cryst. Solids **104**, 203 (1988).
[33] M. Kobayashi and H. Tanaka, Phys. Rev. Lett. **106**, 125703 (2011).
[34] J. L. Aragones, M. Rovere, C. Vega, and P. Gallo, J. Phys. Chem. B **118**, 7680 (2014).
[35] S. Santucci, L. Comez, F. Scarponi, G. Monaco, R. Verbeni, J. F. Legrand, C. Masciovecchio, A. Gessini, and D. Fioretto, J. Chem. Phys. **131**, 154507 (2009).
[36] L. Comez, C. Masciovecchio, G. Monaco, and D. Fioretto, in *Solid State Physics*, edited by R. E. Camley and R. L. Stamps (Academic Press, 2012), Vol. 63, pp. 1–77.
[37] W. Götze, *Complex Dynamics of Glass-Forming Liquids: A Mode-Coupling Theory* (Oxford University Press, Oxford, 2009).
[38] I. S. Joung and T. E. Cheatham, J. Phys. Chem. B **112**, 9020 (2008).
[39] J. L. F. Abascal and C. Vega, J. Chem. Phys. **123**, 234505 (2005).
[40] C. Vega, J. L. Abascal, M. Conde, and J. Aragones, Faraday Discuss. **141**, 251 (2009).
[41] H. J. C. Berendsen, J. P. M. Postma, W. F. van Gunsteren, A. DiNola, and J. R. Haak, J. Chem. Phys. **81**, 3684 (1984).
[42] S. Pronk, S. Páll, R. Schulz, P. Larsson, P. Bjelkmar, R. Apostolov, M. R. Shirts, J. C. Smith, P. M. Kasson, D. van der Spoel, B. Hess, and E. Lindahl, Bioinformatics **29**, 845 (2013).
[43] P. Gallo, F. Sciortino, P. Tartaglia, and S.-H. Chen, Phys. Rev. Lett. **76**, 2730 (1996).
[44] F. Sciortino, P. Gallo, P. Tartaglia, and S.-H. Chen, Phys. Rev. E **54**, 6331 (1996).
[45] M. De Marzio, G. Camisasca, M. Rovere, and P. Gallo, J. Chem. Phys. **144**, 074503 (2016).
[46] M. De Marzio, G. Camisasca, M. Rovere, and P. Gallo, J. Chem. Phys. **146**, 084502 (2017).
[47] Z. Wang, K.-H. Liu, P. Le, M. Li, W.-S. Chiang, J. B. Leao, J. R. D. Copley, M. Tyagi, A. Podlesnyak, A. I. Kolesnikov, C.-Y. Mou, and S.-H. Chen, Phys. Rev. Lett. **112**, 237802 (2014).
[48] P. Gallo and M. Rovere, J. Chem. Phys. **137**, 164503 (2012).
[49] G. Adam and J. H. Gibbs, J. Chem. Phys. **43**, 139 (1965).
[50] C. A. Angell, Chem. Rev. **102**, 2627 (2002).
[51] E. Mamontov and M. Ohl, Phys. Chem. Chem. Phys. **15**, 10732 (2013).
[52] P. Gallo, D. Corradini, and M. Rovere, J. Chem. Phys. **139**, 204503 (2013).
[53] B. Prével, J. Dupuy-Philon, J. F. Jal, J. F. Legrand, and P. Chieux, J. Phys.: Condens. Matter **6**, 1279 (1994).
[54] D. A. Turton, C. Corsaro, M. Candelaresi, A. Brownlie, K. R. Seddon, F. Mallamace, and K. Wynne, Faraday Discuss. **150**, 493 (2011).
[55] M. Conde, M. Rovere, and P. Gallo, Phys. Chem. Chem. Phys. **19**, 9566 (2017).
[56] B. Prevel, J. F. Jal, J. Dupuy-Philon, and A. Soper, J. Chem. Phys. **103**, 1886 (1995).
[57] E. Shiratani and M. Sasai, J. Chem. Phys. **108**, 3264 (1998).
[58] E. Shiratani and M. Sasai, J. Chem. Phys. **104**, 7671 (1996).
[59] K. T. Wikfeldt, A. Nilsson, and L. G. M. Pettersson, Phys. Chem. Chem. Phys. **13**, 19918 (2011).
[60] S. R. Accordino, J. A. Rodriguez Fris, F. Sciortino, and G. A. Appignanesi, Eur. Phys. J. E **34**, 48 (2011).
[61] G. A. Appignanesi, J. A. Rodriguez Fris, and F. Sciortino, Eur. Phys. J. E **29**, 305 (2009).
[62] L. G. M. Pettersson and A. Nilsson, J. Non-Cryst. Solids **407**, 399 (2015).